3D-printable composites for magnetic refrigeration based on Ni-Mn-In-Co magnetic shape memory alloys

V. Sánchez-Alarcos

vicente.sanchez@unavarra.es

Universidad Pública de Navarra

D. L. R. Khanna

Universidad Pública de Navarra

P. La Roca

Bariloche Atomic Centre

V. Recarte

Universidad Pública de Navarra

F. D. Lambri

CONICET-UNR, Ingeniería y Agrimensura

F. G. Bonifacich

CONICET-UNR, Ingeniería y Agrimensura

O. A. Lambri

CONICET-UNR, Ingeniería y Agrimensura

I. Royo-Silvestre

Universidad Pública de Navarra

A. Urbina

Universidad Pública de Navarra

J. I. Pérez-Landazábal

Universidad Pública de Navarra

Research Article

Keywords: Magnetic composite, Metamagnetic shape memory alloy, Polycaprolactone, Fused deposition modelling, Magnetic refrigeration

Posted Date: January 10th, 2024

DOI: https://doi.org/10.21203/rs.3.rs-3787690/v1

Additional Declarations: No competing interests reported.

3D-printable composites for magnetic refrigeration based on Ni-Mn-In-Co magnetic shape memory alloys

V. Sánchez-Alarcos[1,2*], D. L. R. Khanna[1,2], P. La Roca[3], V. Recarte[1,2], F. D. Lambri[4], F. G. Bonifacich[4], O. A. Lambri[4], I. Royo-Silvestre [1,2], A. Urbina[1,2], J. I. Pérez-Landazábal[1,2].

[1]*Department of Physics, Universidad Pública de Navarra, Campus de Arrosadia, 31006 Pamplona, Spain*
[2]*Institute for Advanced Materials and Mathmatics (INAMAT[2]), Universidad Pública de Navarra, Campus de Arrosadia, 31006 Pamplona, Spain*
[3]*Centro Atómico Bariloche (CNEA), CONICET, 8400 Bariloche, Argentina*
[4]*CONICET-UNR. Laboratorio de Materiales, Escuela de Ingeniería Eléctrica, Facultad de Ciencias Exactas, Ingeniería y Agrimensura, Avda. Pellegrini 250, (2000), Rosario, Argentina*

*corresponding author: vicente.sanchez@unavarra.es

Abstract

A high filling load (62% weight) printable magnetic composite has been successfully elaborated from the dispersion of $Ni_{45}Mn_{36.7}In_{13.3}Co_5$ alloy microparticles into a PCL polymer matrix. The composite material has been prepared by solution method, resulting in a very homogeneous particles dispersion into the matrix. The structural transitions in the polymer do not seem to be affected by the addition of the metallic microparticles, which in turn results in a significant increase of the mechanical consistency. The good ductility of the elaborated composite allows its extrusion in flexible printable filaments, from which 3D pieces with complex geometries has been grown. The high measured magnetocaloric response of the composite and the possibility to print high surface/volume ratio geometries make this material a promising candidate for the development of heat exchangers for clean and efficient magnetic refrigeration applications. Furthermore, numerical simulations confirm that, in terms of heat transference, a bulk Ni-Mn-In-Co cubic piece may be even less efficient than a PCL/Ni-Mn-In-Co wire containing the same amount of magnetic active material.

Keywords: Magnetic composite, Metamagnetic shape memory alloy, Polycaprolactone, Fused deposition modelling, Magnetic refrigeration

1. INTRODUCTION

Nowadays, refrigeration plays a crucial role, not only in terms of comfort (e.g. air conditioning) but also for many key aspects of our modern life, such as food and medicine conservation, cooling of electronic devices, etc...[1] Some estimations quantify between 15% and 30% the share of the total worldwide electricity consumption used for refrigeration and air conditioning [2]. A significant reduction of the energy consumption and the replacement of harmful gases required by the traditional vapor compression technology are the main challenges for the refrigeration industry [3]. In this respect, magnetic refrigeration through the magnetocaloric effect (MCE) is considered as a viable clean and energy-efficient alternative technology [4–7].

MCE occurs in all ferromagnetic materials, but it becomes strongly intensified by a phase transition (giant MCE), as observed first in Gd5Si2Ge2 [8]. Among magnetocaloric materials, metamagnetic shape memory alloy (MSMA) stand out due to the giant inverse magnetocaloric effect they show, enhanced by the latent heat of a field-induced martensitic transformation [9–11]. If one considers the figure of merit $\eta = \left| Q/W \right|$ introduced by X. Moya et al [12] (where W is the amount of work needed to drive the caloric effect and Q is the heat exchanged with the thermal bath), Ni-Mn-In-Co alloys present the highest values of η compared to other magnetocaloric materials. Unfortunately, bulk polycrystalline Ni-Mn-In-Co alloys are very brittle and suffer from rapid failure upon repetitive thermal or mechanical cycling. This is an important drawback, as long-term cycling of the material is inherent to the solid-state refrigeration. To tackle this problem, usage of the functional material in powder form (with micro or nanosized particles) consolidated in a polymer matrix to form a composite has been considered as an alternative to the pure bulk material, since the polymer may give structural integrity and formability while the particles provide magneto-thermal functionality [13–15].

On the other hand, for any magnetic refrigeration applications, the design of well-controlled geometries of heat exchangers (increased surface to volume ratio) is crucial to obtain a good performance and efficiency in the heat transfer between the active material and the surroundings [16]. In this sense, if functional Ni-Mn-In-Co particles are embedded in printable thermoplastic polymers, the obtained composite material could be also used to feed a standard Fused Deposition Modelling (FDM) 3D printer, which would allow the growth of complex geometries otherwise not achievable from the brittle bulk. Moreover, the relatively low extruding temperatures used in FDM prevent the possible deterioration of the physical properties of the metallic particles, contrary to what occurs in Selective Laser or Electron Beam Melting techniques used for direct 3D printing of metallic materials, in which the melting and the rapid solidification of the material modify the microstructure with undesired phases and introduce both composition gradients and strong texture [16–19].

The inclusion of magnetic particles in 3D printable polymer matrix composites has been intensively studied during last years in the seek for new integrated functionalities. Nanoparticles of ferrites are, by far, the most used active material to incorporate magnetic action on 3D printed polymeric devices. For instance, soft actuators based on magneto-sensitive materials with outstanding magnetic-control performance and able to actuate under several stimuli (temperature, light, magnetic field,…) have been widely developed for applications in industrial, medical and other fields [20–23]. On the other hand, the feasibility of the production of permanent magnets by 3D printing, using composites made of magnetic microparticles of MnAl-based alloys in a polymer matrix, has been shown by E. Palmero et al [24–27]. In a similar way, the suitability of the use of a 3D printable magnetic composites (magnetocaloric (La,Ce)(Fe,Mn,Si)13–H particles in a PLA matrix) for magnetic refrigeration applications has been very recently confirmed [28]. Nevertheless, the elaboration of printable magnetic

composites based on Ni-Mn-In-Co alloys, which, apart from its large and very efficient magnetocaloric effect, are free of rare-earths, precious, expensive, toxic or non-earth abundant elements [11], remains in turn unexplored.

In order to obtain polymer-based composites suitable for the development of magnetocaloric devices, high filler loadings are desirable to partially offset the inherent low thermal conductivity of the polymers. Polycaprolactone (PCL) showing low melting point and high ductility close to ambient temperature appears as a good candidate for the development of high filling-factor composites for MCE applications [29–31]. On this basis, in the present work a Ni-Mn-In-Co/PCL magnetic composite with a high proportion of active microparticles (MPs), able to feed standard and cheap FDM 3D printers, has been elaborated and characterized. In spite of the thermal conductivity is highly reduced due to the presence of the polymeric material, numerical simulations performed before elaboration show the feasibility of using FSMA-PCL polymeric composites as heat exchangers for magnetic cooling devices. Composites with filler load close to 70% have been successfully extruded in flexible printable filaments, from which 3D pieces with complex geometries could be grown. From the analysis of its thermal, mechanical and magnetic properties (in particular, magnetocaloric effect), the elaborated material appears as a promising candidate for the development of heat exchangers for magnetic refrigeration applications.

2. MATERIALS AND METHODS

2.1 Numerical simulations

The suitability of using PCL/Ni-Mn-In-Co composites as heat exchangers in magnetic cooling devices has been preliminary analyzed from numeric calculations. In particular, finite element simulations have been peformed to compare the heat transfer kinetics of cubic pieces

of pure Ni-Mn-In-Co with that of composite wires containing the same amount of active material. Simulated wires were cylindrical (0.6 mm diameter -same as our FDM printer nozzle- and 600 mm length) and spherical MPs with an average diameter of 85 μm were randomly distributed along the wires, the initial temperature of the particles being 5 K higher than that of the surrounding (polymer matrix and environment, assumed to be initially at room temperature, RT). The cross section of the wire borders was modelled using an adiabatic (Neumann) boundary condition to avoid heat transfer along the axis of the wire. Energy balances were calculated by a homebrew 3D FEM transient heat-transfer simulation, meshing was done via Gmsh (an OpenSource mesh generator) and the simulation code was implemented via Matlab.

Simulations calculate the dynamics of the thermal energy transfer towards or from the surroundings, the transfer rating being dependent on the length of the wire, percentage of particles, quality of cooling/heat transfer to the medium and material properties (thermal conductivity, K, specific heat, Ce, and density, ρ). Ni-Mn-In-Co MPs were assigned to subdomain 1 and PCL to subdomain 2, with their corresponding values ρ_1=8100 kg/m^3, ρ_2=1150 kg/m^3, K_1=10 Wm^{-1}/K, K_2=0.2 Wm^{-1}/K, C_{e_1}=478 Jkg^{-1}/K and C_{e_2}=1928 Jkg^{-1}/K. The differential equation for each point in the space is $C_{e_i}\rho_i \frac{\partial T_i}{\partial t} - \nabla \cdot K_i \nabla T_i = 0$ being i the index of the subdomain and $-K_i \nabla T_i \cdot \mathbf{n} = h(T_i - T_{ext})$ the mixed (Robin) boundary condition [32]. The quality of cooling/heat transfer to the surrounding fluid has been modelled through a single convection coefficient, h. The convection coefficient h takes typical values for different conditions of the surrounding fluid. Therefore, h = 50 is suitable for the interface between most materials and stagnant water or air at low velocity, h = 1000 is appropriate for forced convection of water or air, while h = 10^6 (equivalent to the Dirichlet condition) models a perfect refrigeration circuit at high fluid speeds [33].

2.2 Elaboration of Ni-Mn-In-Co microparticles

A $Ni_{45}Mn_{36.7}In_{13.3}Co_5$ alloy (expected to show a giant magnetocaloric effect, even after milling [34,35]) was produced by arc melting from pure elements. The obtained ingot was homogenized at 1170 K during 24 hours and then slowly cooled to room temperature. The bulk alloy was subjected to 15 minutes milling in a Retsch PM-100 planetary ball mill at 300 rpm with a 5:1 ball-to-powder ratio, and those MPs below 100 μm were selected after sieving. No narrower sieve was performed since the mixture of fine and coarse particles has been recently shown to favor the achievement of high filling factors in similar polymer-based magnetic composites [27]. In order to recover the expected degradation of both the MT and the saturation magnetization caused by milling [36,37], the MPs were subjected to a 45 minutes post-mill annealing treatment at 873 K.

2.3 Production of PCL/Ni-Mn-In-Co composites

On the seek for composites with a high fraction of magnetically-active particles, different composites were elaborated from the dispersion of an increasing concentration of the ball-milled MPs into commercial PCL, by solution casting method. The preparation procedure, illustrated in Figure 1, was as follows: one part (in mass) of PCL was diluted in three parts of dichloromethane (DCM) and continuously stirred at RT until a viscous and translucent homogeneous liquid was obtained. The Ni-Mn-In-Co MPs were then added to the liquid, the temperature was increased up to 313 K and the mixture was continuously stirred for around two hours until a homogenous dark solution was reached. The temperature was again increased up to 353K and hexane was incorporated to the dark solution (three times the total weight of the solution) in order to induce the solid-liquid phase separation. The evaporation of DCM increased the hexane/DCM ratio, which in turn helped the precipitation process thus giving rise

to a foam of polymeric matrix with homogeneously distributed MPs inside. The foam was finally dried for an hour at RT.

The highest achieved particle concentration (weight %) compatible with an admissible mechanical consistency (understood as the ability to be extruded in windable filaments) was 70%, above which all the elaborated composites suffered from severe brittleness. All subsequent studies were therefore performed on this PCL_{30}/MPs_{70} high filling factor composite. It is worth noting that the corresponding volume concentration of MPs in the magnetic composite is 25%, which indeed lies inside the concentration range endorsed by the simulations above.

2.4 3D printing

The foam obtained for this specific PCL_{30}/MPs_{70} composite was extruded into continuous and flexible wires using a Felfil Evo extruder with a 1.75-mm circular cross-section nozzle. The magnetic filaments were used to feed an Artillery Sidewinder X1 3D printer based on the FDM technology, from which several 3D objects with different shapes and sizes could be printed. In particular, as shown in Figure 2, a honeycomb maze-like piece was successfully printed as an example of the intricate geometries attainable from this material. Printing was performed at 473 K and a 0.6 mm diameter nozzle was used to prevent head clogging. The bed temperature was 303 K and the printing speed was 12.5 mm/min, slow enough to ensure cooling of previous layers. In all cases, the Open Source-Software CURA 4.12.1 (Ultimaker B.V. Utrecht, Netherlands) was used to format the printing algorithm (layer thickness of 0.3 mm and 100% infill density).

2.5 Characterization

The composition of the elaborated alloy was checked by electron dispersive spectroscopy (EDS) using a Zeiss EVO 15 VP Scanning Electron Microscope (SEM), also used to check the MPs size and to analyze both the distribution of MPs inside the polymer matrix and the surface morphology of the magnetic filaments. The sequence of magnetostructural transitions taking place on both the MPs and the composite were determined from differential scanning calorimetry (Q-100 DSC, TA Instruments), while the thermal stability of the composite was studied from Thermogravimetry Analysis (Mettler Toledo TGA/DSC 3+), measurements carried out in all cases on heating/cooling ramps at 10 K/min. The mechanical properties of the composite were analyzed by Dynamic Mechanical Analysis (DMA) measurements (damping, Q^{-1}, and dynamic shear modulus, G'), carried out in an inverted torsion pendulum, working in forced oscillations at natural frequencies on around 3 Hz, under atmospheric Argon pressure. Damping was determined by measuring the relative half width of the squared resonance peak for a specimen driven into forced vibration, using [14,38]

$$\tan(\phi) = \frac{\omega_2 - \omega_1}{\omega_0} \qquad (1)$$

where ω_0 is the resonant frequency, and ω_1 and ω_2 are the frequencies at which the amplitude of oscillation reduces to $1/\sqrt{2}$ of the maximum value. The samples for DMA were 3D printed parallelepiped bars of around 1 x 3-4 x 15 mm. Finally, the magnetic properties were analyzed from temperature dependence *M(T)* and field dependence *M(H)* magnetization measurements performed by SQUID magnetometry (QD MPMS XL-7). The MCE (specifically, the magnetically-induced isothermal entropy change, ΔS_{iso}) was estimated from a set of magnetization curves measured on heating under different magnetic fields ranging from 100Oe to 60 kOe, following the expression $\Delta S_{iso} = S(T,H) - S(T,O) = \int_0^H \left(\frac{\partial M}{\partial T}\right)_H dH$ [39]

3. RESULTS AND DISCUSSION

Figure 3 shows the remaining thermal energy in the material (Main panel: normalized, Inset: absolute values) as a function of time for composite wires made up from PCL matrix and 10%, 30% and 50% volume fraction of functional MPs, together with the corresponding curves for the corresponding bulk Ni-Mn-In-Co pieces (2.6 mm, 3.7 mm and 4.4 mm cubes, respectively). It is worth noting that, despite the low thermal conductivity of the polymer matrix, in all cases and for all convection regimes (poor/passive, normal/forced and perfect) the thermal energy transfer is much faster in the wires than in the corresponding bulk cubes. In particular, under passive or forced transfer conditions, it takes up to 15 times less time for the 30% and 50% wires to transfer heat compared to the respective cubes, which means a very relevant improvement of the heat transference velocity. Nevertheless, the absolute energy transferred is also important since larger quantities of heat transferred in short times results in a higher transference efficiency. So, the ratio between the initial energy and the time (τ) required to reduce to 1% the initial stored energy, $\eta = Q_i/\tau$, can be a useful indicator to assess the ability of the composite to transfer heat from the source (active material) to the refrigeration fluid. Table 1 shows the calculated values of both the transfer time and η, the latter presented both per volume of active material ($\rho_\eta^{act} = \eta/V_{act}$) and per total volume ($\rho_\eta^{tot} = \eta/V_{tot}$) in order to better compare. As expected, the larger is the cube size the lower is the ability of the active material to transfer heat from the source. However, interestingly, wires make better use of the active material since more energy per second is transferred for the same amount of used alloy (except for the particular case of 10% MP composites working under perfect convection). What is more, wires with 30% and 50% of MPs make better use even of the total material volume, compared to the corresponding cubic bulk piece. Therefore, it seems that not only the heat transfer quickness but also the harnessing of magnetic material, available space and net mass

would be better in the composite wires than in the alloy cubes. Hence, the numerical results support the idea that PCL/Ni-Mn-In-Co composites with high specific surface can be even more efficient than a standard Ni-Mn-In-Co metallic piece in terms of heat transference, which does indeed encourage the fabrication of printable functional PCL/Ni-Mn-In-Co composites for magnetocaloric applications.

Regarding the elaborated alloy, Figure 4 shows the DSC thermogram obtained on heating/cooling between 230 K and 400 K the just sieved Ni-Mn-In-Co MPs. The observed exothermic and endothermic peaks evidence the occurrence of a reversible MT just below RT, showing the typical thermal hysteresis. The MCE linked to the magnetic-field induction of such MT is shown in the upper inset as a function of both temperature and applied field. A net highest ΔS_{is} value of 8 J/kgK is achieved at around 270 K, temperature at which the reverse MT takes place under 6 T. Even though this value is far from the highest values obtained in some similar bulk alloys [40], the broadening of the peak temperature range (ΔT) as a consequence of the milling-induced deformation results in a very large Refrigeration Cooling Power, $RCP \approx \Delta S_{iso} \cdot \Delta T$, which is indeed the main performance metric to rank magnetocaloric materials [41]. In particular, a $RCP = 380\, J/kg$ is obtained for the MPs under a 6 T applied field, close to the higher values reported up to now in literature for this alloys system [40]. The elaborated particles show therefore both small sizes compatible with the extruder nozzles (see lower inset) and a huge MCE response, thus meeting the two main requirements to be used as a magnetically-active material in printable composites for magnetic refrigeration applications.

The microstructure of the PCL_{30}/MPs_{70} elaborated magnetic composite has been analyzed from SEM observations. Figure 5 shows the micrographs obtained in a longitudinal section of a freshly extruded composite filament. A very homogeneous dispersion of the MPs is observed all along the studied filaments, which show a quite regular diameter of 1.5 ± 0.2 mm. The high

homogeneity of the MPs dispersion is even more evident in the Ni mapping image, where deeper particles can be also detected. This seems to confirm that no significant agglomeration of particles occurred neither during the composite elaboration nor because of the extrusion process. As previously mentioned, such a proper distribution of particles with different sizes could be behind the successfully achieved combination of high filling-factor and high ductility [27].

The DSC thermogram obtained on heating/cooling a sample of the extruded filament is shown in Figure 6a. As indicated, the very large endothermic peak observed around 330 K corresponds to the melting of the PCL matrix whereas the exothermic one around 300 K is linked to the polymer crystallization taking place on subsequent cooling. The calculated enthalpies for melting and crystallization in the composite are 25.0 J/g and 26.4 J/g, respectively, which in both cases represent around 38% of the pure PCL enthalpies ($\Delta H_{melt}^{PCL} = 66 J/g$ and $\Delta H_{cryst}^{PCL} = 69 J/g$ [31]), a slightly higher value than the nominal 30% PCL weight concentration. On the other hand, the much smaller enthalpy change associated to the MT in the metallic MPs (~ 20 times lower) makes the corresponding peaks to be hardly detected in the thermogram. Interestingly, the melting and crystallization temperatures in the composite are very close to those in pure PCL (whose thermogram has been rescaled in the graph for the sake of clarity), pointing out a very small influence of the presence of the particles on the structural transitions in the polymer.

In order to check the composition of the elaborated composite, TGA measurements were performed on two different composite samples, extracted from the beginning and the end of the extruded wire. Figure 6b shows the temperature dependence of weight (percentage) measured on heating both the composite and pure PCL samples from RT up to 900 K. The weight losses observed between 600 K and 750 K correspond to the PCL decomposition, in such a way the

mass fraction of MPs on the composite can be directly determined as the remnant mass percentage at the end of the thermal scan. The MPs concentration thus obtained is around 62%, in perfect agreement with that inferred from the melting and crystallization enthalpy values. The fact that the actual MPs concentration is lower than the nominal concentration could be due to some unwanted mixing of the extra PCL added as a pushing agent in the extruder (in order to be able to extract all the introduced composite material). In any case, the same final mass fraction is observed for the two composite samples, which confirms a very high degree of homogeneity on the particles dispersion along the filament. A considerable shift of the PCL decomposition to lower temperatures is, in turn, observed as a consequence of the addition of MPs. This is in accordance with previous results [31,42,43] where the increase in the pyrolysis of PCL chains has been ascribed to the limitation of the movement of polymeric chains caused by the incorporation of magnetic particles. Nevertheless, the composite decomposition is well above the usual printing temperatures in FDM 3D printing, so no influence whatsoever is expected in any elaboration or operation step.

The effect of the metallic fillers on the mechanical response of the material has been analyzed from DMA measurements performed on two identical parallelepiped samples 3D printed from both the composite and pure PCL. As shown in Figure 7, the dynamical modulus around RT (expected working temperatures) is much higher in the composite, which means a greater stiffness and therefore an increased mechanical consistency as a result of the metallic particles addition, in accordance with the rule-of-mixture models [44,45]. Such behavior could be also related to the associated decrease in the mobility of the polymer chains, as already proposed in similar composites [46]. On the other hand, although no significant modulus defect is observed linked to the occurrence of the MT in the metallic MPs, a well-defined damping peak is indeed clearly detected in the internal friction measurement, as shown in the inset. This

is quite interesting since it confers the material an extra damping capacity at RT which may be useful to mitigate the impact of low frequency mechanical vibration in the printed devices.

The magnetic properties of the composite have been tested in a small piece cut from a 3D printed sample. In order to better compare, the measured magnetization is shown in Figure 8a as a function of the applied magnetic field both for the alloy MPs and for the composite sample. The overall behavior is the same and, as expected, just a net decrease in magnetization is observed because of the reduced amount of magnetic material. In particular, the magnetizations values under a 6 T applied field (which could be assimilated to saturation magnetization) are 51.6 emu/g and 82.5 emu/g for the composite and the MPs, respectively, in perfect agreement with the above-mentioned estimation of 62% of MPs in the wire. This matching is quite relevant as it means that the concentration of particles in the composite has not been affected at all by the FDM printing process. Finally, the magnetic refrigeration capacity of the composite has been assessed from the estimation of the MCE. Figure 8b show the temperature and field dependence of ΔS_{iso}, obtained from the corresponding magnetization measurements in the printed sample. A highest ΔS_{iso} value of 3.8 J/kgK is obtained at 6 T, which results in a RCP ≈ 200 J/kg, an endorsing value for the elaboration of heat-exchanger for magnetic refrigeration applications.

4. CONCLUSSIONS

A high filling load printable magnetic composite has been successfully elaborated from the dispersion of $Ni_{45}Mn_{36.7}In_{13.3}Co_5$ alloy microparticles into a PCL polymer matrix. The composite material has been prepared by solution method, resulting in very homogeneous particles dispersion. The good ductility of the elaborated composite allows its extrusion in

flexible printable filaments, from which 3D pieces with complex geometries has been grown. The structural transitions in the polymer does not seem to be affected by the addition of the metallic microparticles, which in turn results in a significant increase of the mechanical consistency. The high measured magnetocaloric response, together with the support of numerical simulations confirming that PCL/Ni-Mn-In-Co wires can be even more efficient than a corresponding Ni-Mn-In-Co metallic cube in terms of heat transference, make this material a promising candidate for the development of heat exchangers for clean and efficient magnetic refrigeration applications

Authors contribution

Vicente Sánchez-Alarcos, Deepali Khanna and Paulo La Roca conceived this research, elaborated the material and designed experiments. Fernando Daniel Lambri, Federico Guillermo Bonifacich and Osvaldo Agustín Lambri elaborated samples, carried out measurements and performed both analysis and interpretation of data from DMA. Isaac Royo-Silvestre performed numerical simulation. José Ignacio Pérez-Landazábal and Vicente Recarte performed and interpreted thermal and magnetic measurements. Antonio Urbina performed microstructural characterization. Vicente Sánchez-Alarcos wrote the paper and participated in its revision. All authors participated in the interpretation of the data, and they all revised and approved the final manuscript.

Funding

This work has been carried out with the financial support of the Spanish "Ministerio de Ciencia e Innovación" (PID2022-138108OB-C32, MCIN/AEI/10.13039/501100011033/FEDER, UE), the CONICET-PIP 11220210100073CO (2022-2024), the PPCT–UNR 80020220600018UR (2023-2026) and the PID-UNR 80020220700026UR (2023-2026) projects.

Conflict of Interest

The authors declare that they have no conflict of interest.

Data availability statement

The authors confirm that the data supporting the findings of this study are available within the article.

References

[1] IEA, The Future of Cooling: Opportunities for energy-efficient air conditioning, Paris, 2018. https://www.iea.org/reports/the-future-of-cooling.
[2] N.K. Shah, N. Khanna, N. Karali, W. Park, Y. Qu, N. Zhou, Opportunities for simultaneous efficiency improvement and refrigerant transition in air conditioning, (2017).
[3] D. Coulomb, Refrigeration and cold chain serving the global food industry and creating a better future: two key IIR challenges for improved health and environment, Trends in Food Science & Technology. 19 (2008) 413–417. https://doi.org/10.1016/j.tifs.2008.03.006.
[4] J. Liu, T. Gottschall, K.P. Skokov, J.D. Moore, O. Gutfleisch, Giant magnetocaloric effect driven by structural transitions, Nature Materials. 11 (2012) 620–626. https://doi.org/10.1038/nmat3334.
[5] M.M. Vopson, The multicaloric effect in multiferroic materials, Solid State Communications. 152 (2012) 2067–2070. https://doi.org/10.1016/j.ssc.2012.08.016.
[6] X. Moya, S. Kar-Narayan, N.D. Mathur, Caloric materials near ferroic phase transitions, Nature Materials. 13 (2014) 439–450. https://doi.org/10.1038/nmat3951.
[7] N.A. Zarkevich, D.D. Johnson, V.K. Pecharsky, High-throughput search for caloric materials: the CaloriCool approach, Journal of Physics D: Applied Physics. 51 (2017) 024002. https://doi.org/10.1088/1361-6463/aa9bd0.

[8] V.K. Pecharsky, K.A. Gschneidner Jr., Giant Magnetocaloric Effect in \mathrmGd_5(\mathrmSi_2\mathrmGe_2), Phys. Rev. Lett. 78 (1997) 4494–4497. https://doi.org/10.1103/PhysRevLett.78.4494.
[9] A. Planes, L. Mañosa, M. Acet, Magnetocaloric effect and its relation to shape-memory properties in ferromagnetic Heusler alloys, Journal of Physics: Condensed Matter. 21 (2009) 233201. https://doi.org/10.1088/0953-8984/21/23/233201.
[10] T. Gottschall, A. Gràcia-Condal, M. Fries, A. Taubel, L. Pfeuffer, L. Mañosa, A. Planes, K.P. Skokov, O. Gutfleisch, A multicaloric cooling cycle that exploits thermal hysteresis, Nature Materials. 17 (2018). https://doi.org/10.1038/s41563-018-0166-6.
[11] V. Franco, J.S. Blázquez, J.J. Ipus, J.Y. Law, L.M. Moreno-Ramírez, A. Conde, Magnetocaloric effect: From materials research to refrigeration devices, Progress in Materials Science. 93 (2018) 112–232. https://doi.org/10.1016/j.pmatsci.2017.10.005.
[12] X. Moya, E. Defay, V. Heine, N.D. Mathur, Too cool to work, Nature Physics. 11 (2015) 202–205. https://doi.org/10.1038/nphys3271.
[13] J. Liu, N. Scheerbaum, S. Kauffmann-Weiss, O. Gutfleisch, NiMn-Based Alloys and Composites for Magnetically Controlled Dampers and Actuators, Advanced Engineering Materials. 14 (2012) 653–667. https://doi.org/10.1002/adem.201200038.
[14] F.G. Bonifacich, O.A. Lambri, V. Recarte, V. Sánchez-Alarcos, J.I. Pérez-Landazábal, Magnetically tunable damping in composites for 4D printing, Composites Science and Technology. 201 (2021) 108538. https://doi.org/10.1016/j.compscitech.2020.108538.
[15] B. Rodríguez-Crespo, D. Salazar, S. Lanceros-Méndez, V. Chernenko, Development and magnetocaloric properties of Ni(Co)-Mn-Sn printing ink, Journal of Alloys and Compounds. 917 (2022) 165521. https://doi.org/10.1016/j.jallcom.2022.165521.
[16] D. Jafari, W.W. Wits, The utilization of selective laser melting technology on heat transfer devices for thermal energy conversion applications: A review, Renewable and Sustainable Energy Reviews. 91 (2018) 420–442. https://doi.org/10.1016/j.rser.2018.03.109.
[17] S.H. Masood, W.Q. Song, Development of new metal/polymer materials for rapid tooling using Fused deposition modelling, Materials & Design. 25 (2004) 587–594. https://doi.org/10.1016/j.matdes.2004.02.009.
[18] J.D. Moore, D. Klemm, D. Lindackers, S. Grasemann, R. Träger, J. Eckert, L. Löber, S. Scudino, M. Katter, A. Barcza, K.P. Skokov, O. Gutfleisch, Selective laser melting of La(Fe,Co,Si)13 geometries for magnetic refrigeration, Journal of Applied Physics. 114 (2013) 043907. https://doi.org/10.1063/1.4816465.
[19] M.P. Caputo, A.E. Berkowitz, A. Armstrong, P. Müllner, C.V. Solomon, 4D printing of net shape parts made from Ni-Mn-Ga magnetic shape-memory alloys, Additive Manufacturing. 21 (2018) 579–588. https://doi.org/10.1016/j.addma.2018.03.028.
[20] M.Y. Khalid, Z.U. Arif, R. Noroozi, A. Zolfagharian, M. Bodaghi, 4D printing of shape memory polymer composites: A review on fabrication techniques, applications, and future perspectives, Journal of Manufacturing Processes. 81 (2022) 759–797. https://doi.org/10.1016/j.jmapro.2022.07.035.
[21] E.A. Périgo, J. Jacimovic, F. García Ferré, L.M. Scherf, Additive manufacturing of magnetic materials, Additive Manufacturing. 30 (2019) 100870. https://doi.org/10.1016/j.addma.2019.100870.
[22] G. Shao, H.O.T. Ware, J. Huang, R. Hai, L. Li, C. Sun, 3D printed magnetically-actuating micro-gripper operates in air and water, Additive Manufacturing. 38 (2021) 101834. https://doi.org/10.1016/j.addma.2020.101834.
[23] W. Zhao, Z. Huang, L. Liu, W. Wang, J. Leng, Y. Liu, Bionic design and performance research of tracheal stent based on shape memory polycaprolactone, Composites Science and Technology. 229 (2022) 109671. https://doi.org/10.1016/j.compscitech.2022.109671.
[24] E.M. Palmero, J. Rial, J. de Vicente, J. Camarero, B. Skårman, H. Vidarsson, P.-O. Larsson, A. Bollero, Development of permanent magnet MnAlC/polymer composites and flexible filament for bonding and 3D-printing technologies, Science and Technology of Advanced Materials. 19 (2018) 465–473. https://doi.org/10.1080/14686996.2018.1471321.
[25] E.M. Palmero, D. Casaleiz, N.A. Jiménez, J. Rial, J. de Vicente, A. Nieto, R. Altimira, A. Bollero, Magnetic-Polymer Composites for Bonding and 3D Printing of Permanent Magnets, IEEE Transactions on Magnetics. 55 (2019) 1–4. https://doi.org/10.1109/TMAG.2018.2863560.
[26] E.M. Palmero, A. Bollero, 3D and 4D Printing of Functional and Smart Composite Materials, in: D.B.T.-E. of M.C. Brabazon (Ed.), Elsevier, Oxford, 2021: pp. 402–419. https://doi.org/10.1016/B978-0-12-819724-0.00008-2.
[27] E.M. Palmero, D. Casaleiz, J. de Vicente, B. Skårman, H. Vidarsson, P.-O. Larsson, A. Bollero, Effect of particle size distribution on obtaining novel MnAlC-based permanent magnet composites and flexible

filaments for 3D-printing, Additive Manufacturing. 33 (2020) 101179. https://doi.org/10.1016/j.addma.2020.101179.
[28] Á. Díaz-García, J. Revuelta, L.M. Moreno-Ramírez, J.Y. Law, C. Mayer, V. Franco, Additive manufacturing of magnetocaloric (La,Ce)(Fe,Mn,Si)13–H particles via polymer-based composite filaments, Composites Communications. 35 (2022) 101352. https://doi.org/10.1016/j.coco.2022.101352.
[29] C. Yue, M. Li, Y. Liu, Y. Fang, Y. Song, M. Xu, J. Li, Three-dimensional printing of cellulose nanofibers reinforced PHB/PCL/Fe3O4 magneto-responsive shape memory polymer composites with excellent mechanical properties, Additive Manufacturing. 46 (2021) 102146. https://doi.org/10.1016/j.addma.2021.102146.
[30] E. Özen Öner, M.E. Pekdemir, E. Ercan, Y. Say, M. Kök, Y. Aydoğdu, Novel of (PLA/PCL blend)/Gd2O3 rare earth oxide nanocomposites: Shape memory effect, thermal, magnetic, and mechanical properties, Polymer Composites. 43 (2022) 3096–3103. https://doi.org/10.1002/pc.26602.
[31] I. Galarreta-Rodriguez, A. Lopez-Ortega, E. Garayo, J.J. Beato-López, P. La Roca, V. Sanchez-Alarcos, V. Recarte, C. Gómez-Polo, J.I. Pérez-Landazábal, Magnetically activated 3D printable polylactic acid/polycaprolactone/magnetite composites for magnetic induction heating generation, Advanced Composites and Hybrid Materials. 6 (2023) 102. https://doi.org/10.1007/s42114-023-00687-4.
[32] M. Gockenbach, K. Schmidtke, Newton's law of heating and the heat equation, Involve, a Journal of Mathematics. 2 (2009) 419–437. https://doi.org/DOI: 10.2140/involve.2009.2.419.
[33] P. Kosky, R. Balmer, W. Keat, G. Wise, Chapter 12 - Mechanical Engineering, in: P. Kosky, R. Balmer, W. Keat, G. Wise (Eds.), Exploring Engineering (Third Edition), Academic Press, Boston, 2013: pp. 259–281. https://doi.org/10.1016/B978-0-12-415891-7.00012-1.
[34] J.I. Pérez-Landazábal, V. Sánchez-Alarcos, V. Recarte, O.A. Lambri, F.G. Bonifacich, D.L.R. Khanna, I. Unzueta, J.A. García, F. Plazaola, J. López-García, M. Jimenez Ruiz, J.A. Rodríguez-Velamazán, E. Cesari, Influence of Structural Defects on the Properties of Metamagnetic Shape Memory Alloys, Metals. 10 (2020). https://doi.org/10.3390/met10091131.
[35] D.L.R. Khanna, V. Sánchez-Alarcos, V. Recarte, J.I. Pérez-Landazábal, Correlation between particle size and magnetic properties in soft-milled Ni45Co5Mn34In16 powders, Intermetallics. 130 (2021) 107076. https://doi.org/10.1016/j.intermet.2020.107076.
[36] I. Unzueta, J. López-García, V. Sánchez-Alarcos, V. Recarte, J.I. Pérez-Landazábal, J.A. Rodríguez-Velamazán, J.S. Garitaonandia, J.A. García, F. Plazaola, 119Sn Mössbauer spectroscopy for assessing the local stress and defect state towards the tuning of Ni-Mn-Sn alloys, Applied Physics Letters. 110 (2017) 181908. https://doi.org/10.1063/1.4982630.
[37] J. López-García, I. Unzueta, V. Sánchez-Alarcos, V. Recarte, J.I. Pérez-Landazábal, J.A. Rodríguez-Velamazán, J.A. García, F. Plazaola, Correlation between defects and magneto-structural properties in Ni-Mn-Sn metamagnetic shape memory alloys, Intermetallics. 94 (2018) 133–137. https://doi.org/10.1016/j.intermet.2017.12.028.
[38] Lambri, O. A., A Review on the Problem of Measuring Non-Linear Damping and the Obtainment of Intrinsic Damping, in: C.H.W. : J. Martinez-Mardones, D. Walgraef (Ed.), Materials Instabilities, World Scientific Publishing, New York, 2000: pp. 249–280. https://doi.org/10.1142/9789812793317_0005.
[39] V. Recarte, J.I. Pérez-Landazábal, S. Kustov, E. Cesari, Entropy change linked to the magnetic field induced martensitic transformation in a Ni–Mn–In–Co shape memory alloy, Journal of Applied Physics. 107 (2010) 53501. https://doi.org/10.1063/1.3318491.
[40] P. La Roca, J. López-García, V. Sánchez-Alarcos, V. Recarte, J.A. Rodríguez-Velamazán, J.I. Pérez-Landazábal, Room temperature huge magnetocaloric properties in low hysteresis ordered Cu-doped Ni-Mn-In-Co alloys, Journal of Alloys and Compounds. 922 (2022) 166143. https://doi.org/10.1016/j.jallcom.2022.166143.
[41] A.M. Tishin, Magnetic refrigeration in the low-temperature range, Journal of Applied Physics. 68 (1990) 6480–6484. https://doi.org/10.1063/1.347186.
[42] R. Yang, Chapter 7 - Polymer degradation and stability, in: R. Narain (Ed.), Polymer Science and Nanotechnology, Elsevier, 2020: pp. 125–148. https://doi.org/10.1016/B978-0-12-816806-6.00007-8.
[43] W. Xue, Y. Hu, F. Wang, X. Yang, L. Wang, Fe3O4/ poly(caprolactone) (PCL) electrospun membranes as methylene blue catalyst with high recyclability, Colloids and Surfaces A: Physicochemical and Engineering Aspects. 564 (2019) 115–121. https://doi.org/10.1016/j.colsurfa.2018.12.037.
[44] T. Mura, Micromechanics of defects in solids, Martinus Nijhoff Publishers, New York, NY, 1987.
[45] F.G. Bonifacich, O.A. Lambri, F.D. Lambri, P.B. Bozzano, V. Recarte, V. Sánchez-Alarcos, J.I. Pérez-Landazábal, Analysis of the strain misfit between matrix and inclusions in a magnetically tunable composite, Mechanics of Materials. 162 (2021) 104045. https://doi.org/10.1016/j.mechmat.2021.104045.

[46] M. Heidari-Rarani, M. Rafiee-Afarani, A.M. Zahedi, Mechanical characterization of FDM 3D printing of continuous carbon fiber reinforced PLA composites, Composites Part B: Engineering. 175 (2019) 107147. https://doi.org/10.1016/j.compositesb.2019.107147.

Figure captions

FIG. 1: Schematic representation of the composite preparation procedure.

FIG. 2: Extruded filaments and 3D FDM printed pieces.

FIG. 3: Heat transference as a function of time for composite wires made up from PCL matrix and 10%, 30% and 50% volume fraction of functional MPs, together with the corresponding curves for the equivalent bulk Ni-Mn-In-Co cubic pieces. Main panel: normalized, Inset: absolute values.

FIG. 4: DSC thermogram obtained on the just sieved Ni-Mn-In-Co MPs. Upper inset: MCE as a function of temperature and applied field. Lower inset: SEM micrograph on the powder.

FIG. 5: (a) SEM micrograph on a longitudinal section of the composite wire. (b) Corresponding Ni-mapping image.

FIG. 6: (a) DSC thermogram on a sample of the extruded filament. (b) Temperature dependence of weight (percentage) measured on heating both the composite and pure PCL samples from RT up to 900 K.

FIG. 7: Temperature dependence of dynamical modulus for composite and pure PCL 3D printed samples. Inset: Internal friction as a function of temperature.

FIG. 8: (a) Magnetization of both the MPs and the composite at 300 K, as a function of the applied field. (b) Isothermal magnetically-induced entropy change as a function of temperature and applied magnetic field for the elaborated composite.

Table captions

TAB. 1: Calculated values of transfer time (τ), transferred energy per time and volume of magnetic active material ($\rho_{\eta}^{act} = \eta/V_{act}$), and transferred energy per time and total volume ($\rho_{\eta}^{tot} = \eta/V_{tot}$), both for the composite wires and the corresponding metallic cubic pieces.

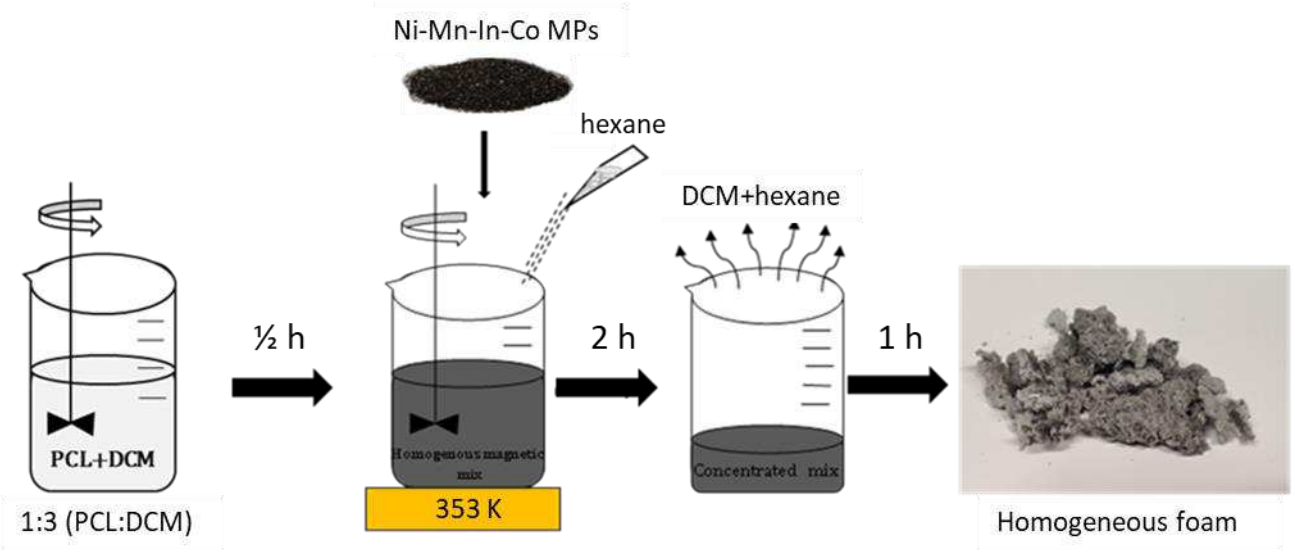

Fig.1

Sánchez-Alarcos et al.

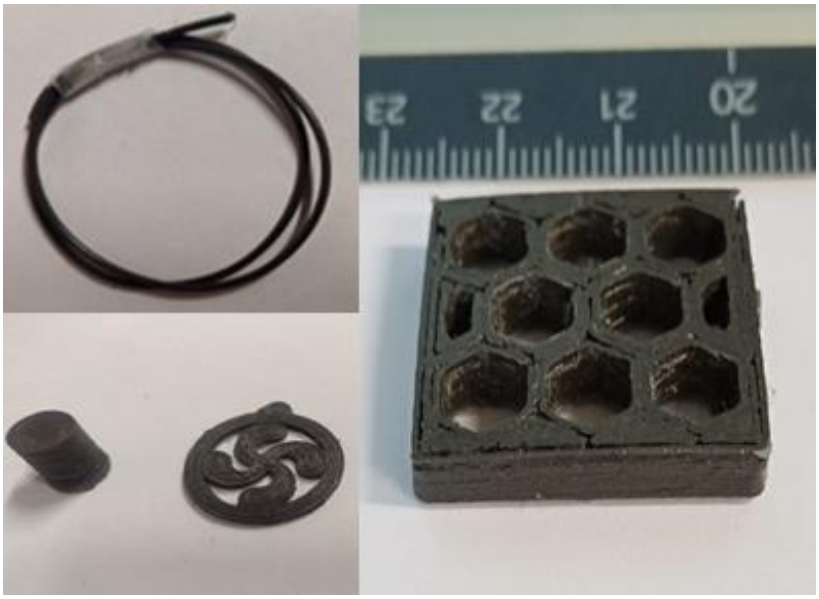

Fig.2

Sánchez-Alarcos et al.

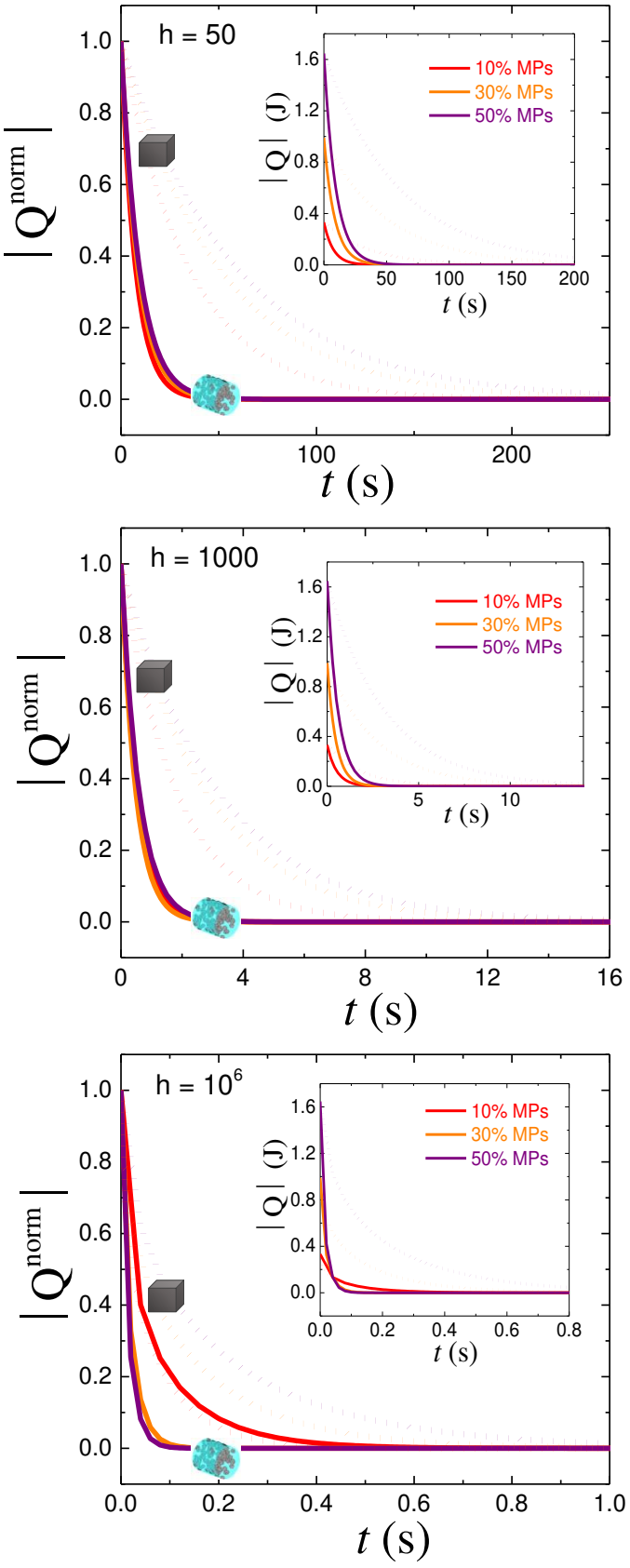

Fig.3

Sánchez-Alarcos et al.

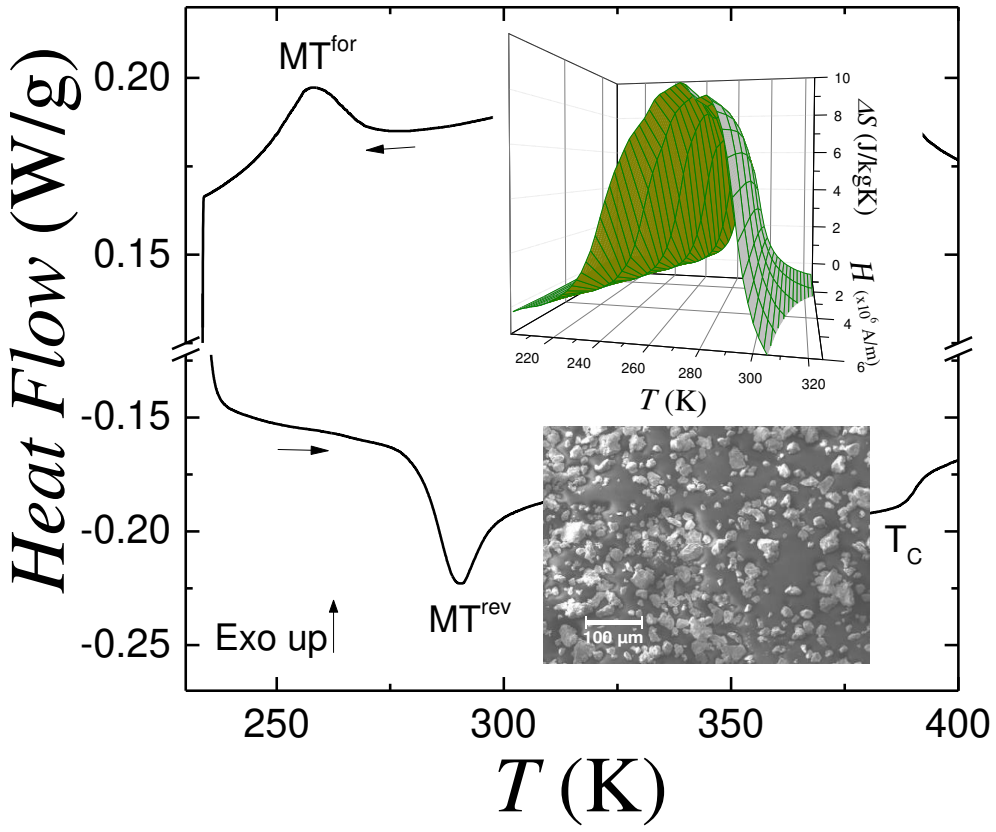

Fig.4

Sánchez-Alarcos et al.

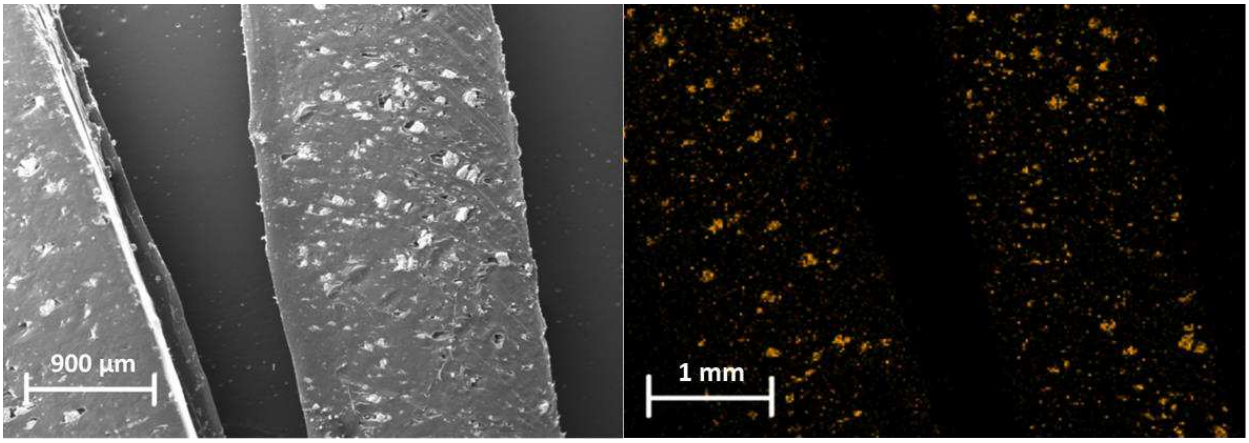

Fig.5

Sánchez-Alarcos et al.

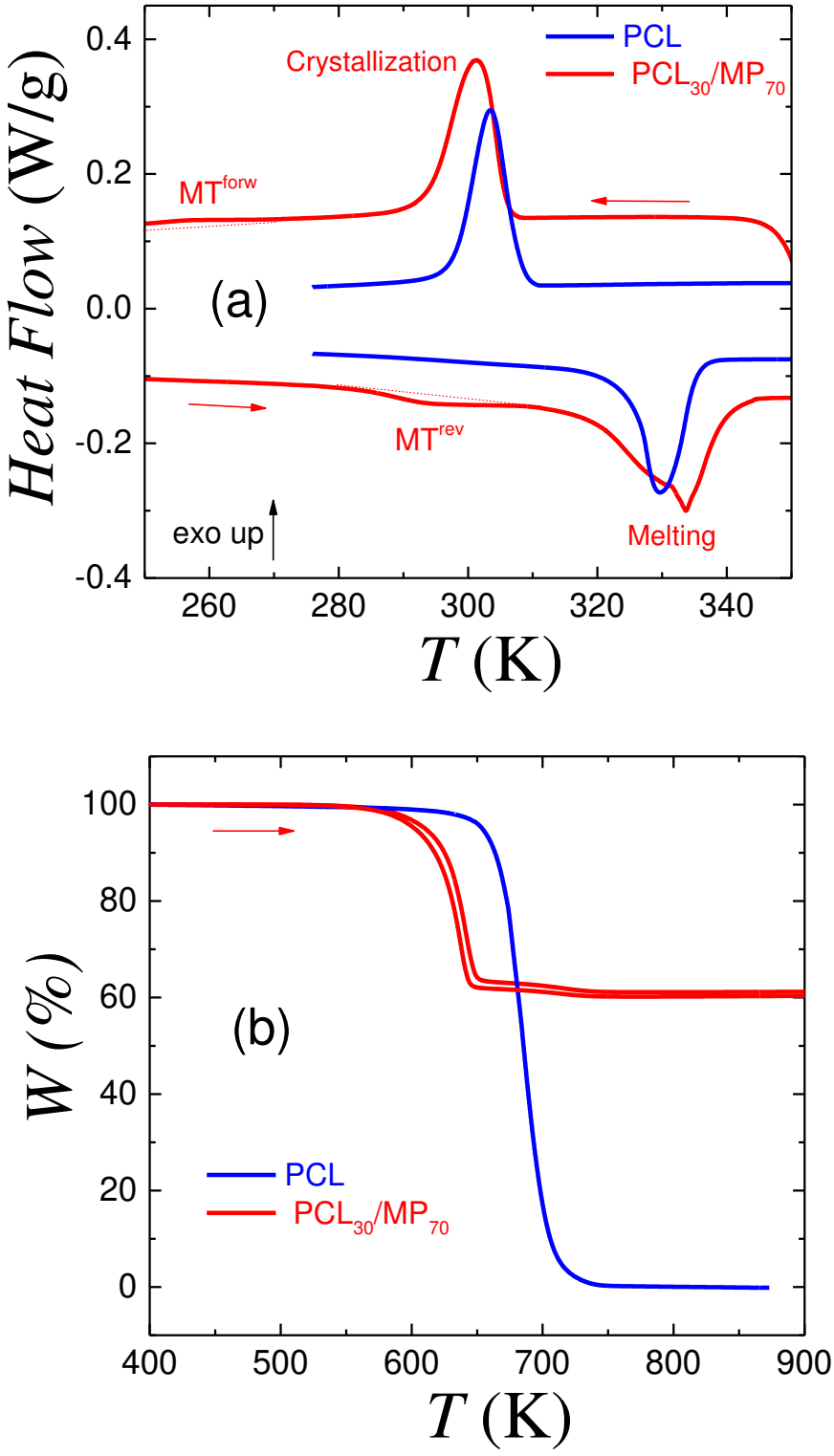

Fig.6

Sánchez-Alarcos et al.

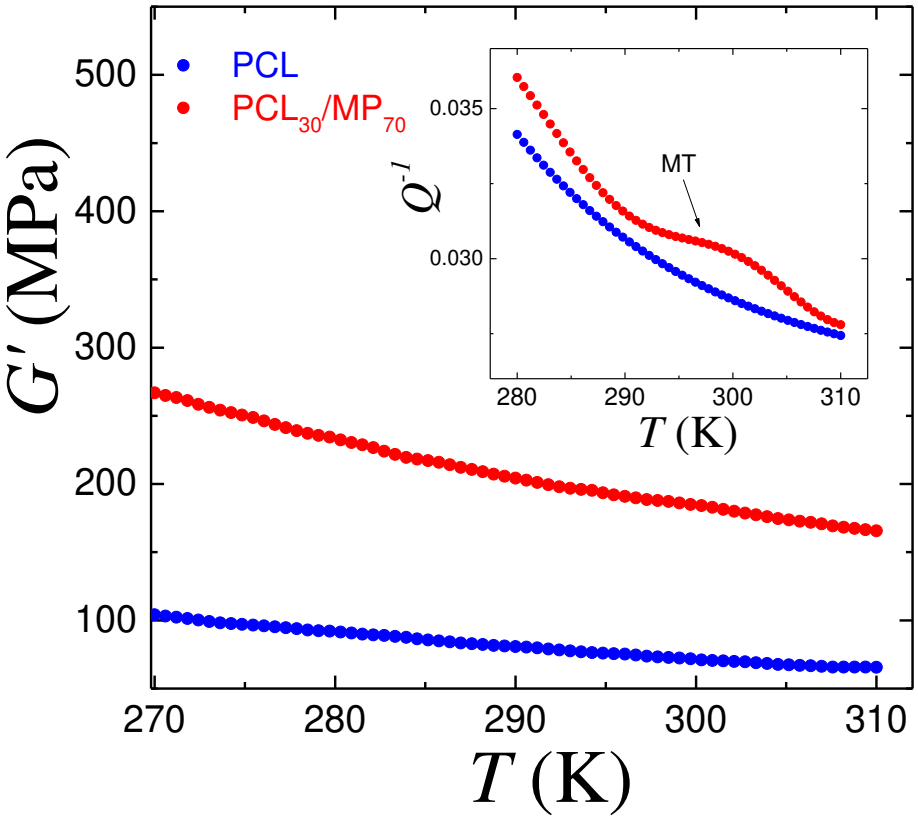

Fig.7

Sánchez-Alarcos et al.

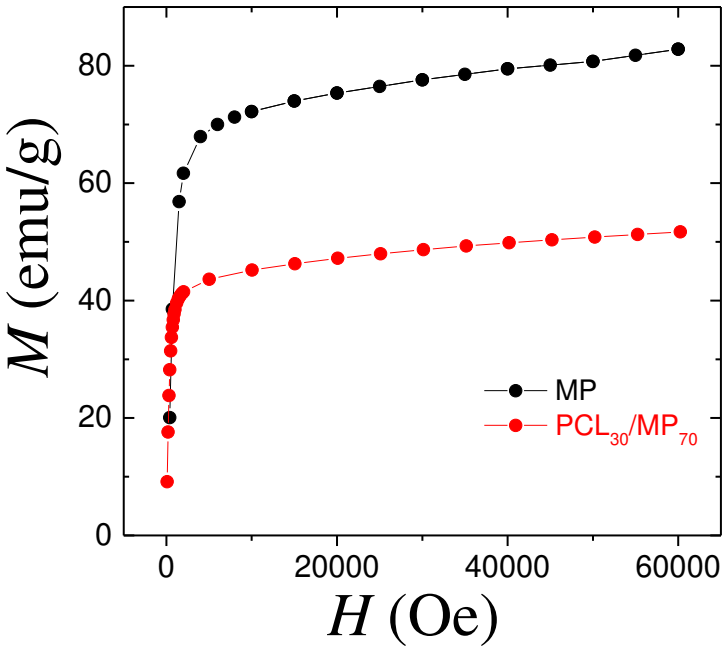

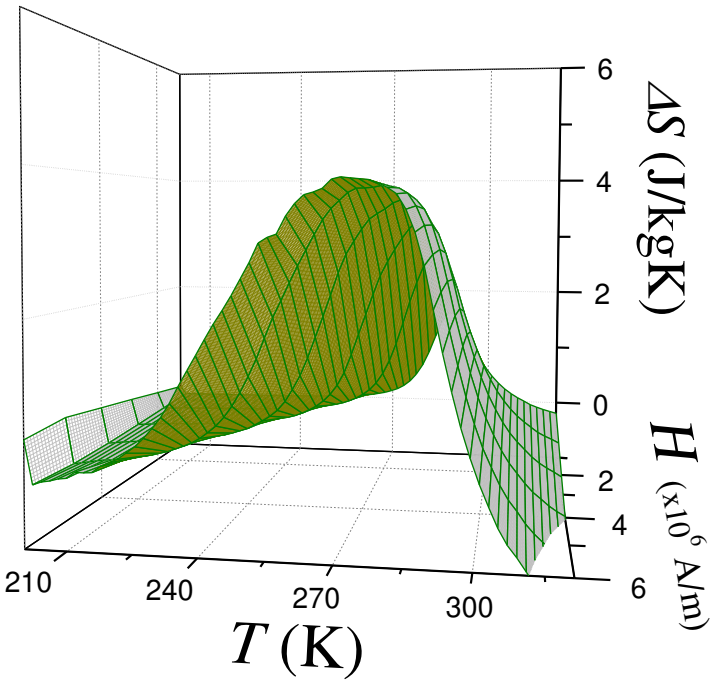

Fig.8

Sánchez-Alarcos et al.

Refrigeration regime	Wire				Cube		
	MP (% vol)	τ (s)	ρ_η^{act} x10^5 (J/sm^3)	ρ_η^{tot} x10^5 (J/sm^3)	Side (mm)	τ (s)	$\rho_\eta^{act} = \rho_\eta^{tot}$ x10^5 (J/sm^3)
h = 50 (Poor)	10	34.01	5,62	0,56	2.6	159.00	1,21
	30	39.83	4,86	1,46	3.7	229.70	0,84
	50	43.26	4,48	2,24	4.4	271.58	0,71
h = 1000 (Normal)	10	2.46	78,6	7,86	2.6	8.28	23,4
	30	2.21	87,7	26,3	3.7	12.57	15,4
	50	2.68	72,2	36,1	4.4	14.48	13,4
h = 10^6 (Perfect)	10	0.44	433	43,3	2.6	0.35	539
	30	0.10	1860	559	3.7	0.72	268
	50	0.07	2450	1220	4.4	1.06	181

Table 1

Sánchez-Alarcos et al.